# SAM overview

Prepared by: *A. Tokovinin*
Revised by: *B. Gregory, D. Sprayberry*
Version: 2
Date: November 7, 2005
File: pdr/overview/overview.tex

## 1 Introduction

For all astronomical instruments, there is an interplay between science drivers, technical opportunities and available resources. In an environment where 8-m telescopes with state-of-the-art AO systems operating in the near IR are becoming common, a strategy for a modern 4-m telescope like SOAR [1] is to exploit a science niche that is not accessed by those telescopes. Such a niche is adaptive optics (AO) in the visible wavelength band.

The concept of the SOAR Adaptive Module, SAM [6, 8], is based on a partial compensation of turbulence at low altitudes, dubbed Ground-Layer Adaptive Optics (GLAO). Unlike classical AO, we do not reach diffraction-limited resolution, but, instead, improve the atmospheric image quality. This improvement extends to the visible wavelengths and works for moderately large fields of several arcminutes. Thus, all classical astronomical programs (except wide-field imagery) can benefit from this correction. This is particularly important for SOAR, destined to reach the highest possible resolution over moderate fields.

The GLAO concept was put forward by F. Rigaut in 2001. The power of GLAO is being recognized by the astronomical community and has led to several ongoing projects: GLAS at WHT [4], MUSE at ESO and Gemini GLAO, for example. Any GLAO system has to preferentially sense ground-layer turbulence using some form of tomography. There are several ways to do this: to average signals from many widely spaced natural guide stars (NGS), as proposed for the Magellan telescopes, use several Rayleigh or sodium laser guide stars (LGS), as in MUSE and Gemini GLAO, or use a single Rayleigh LGS at low altitude, as in SAM and GLAS. The conical beam from a low-altitude beacon naturally senses low turbulent layers with higher weight, hence it is a first-order solution for GLAO. Numerous simulations show that this simple (albeit non-optimal) technique offers interesting performance, which SAM is designed to exploit.

The purpose of this document is to give an introduction to the SAM design. We begin by describing the instrument and its sub-systems, underlining the progress achieved since Conceptual Design reviews but not going into details (cf. Sect. 8). The reader is referred to the many SAM System Design Notes (SDN) for detailed information on the design and trade studies. A special section is devoted to the LGS sub-system, not yet designed in detail. Finally, an update of the expected SAM performance is given that incorporates specific instrument parameters and error budget.

## 2 SAM at a glance

Figure 1 illustrates the overall configuration of the SAM with a schematic indication of the location and interconnections of the sub-systems. The SAM can be conveniently broken down into four major

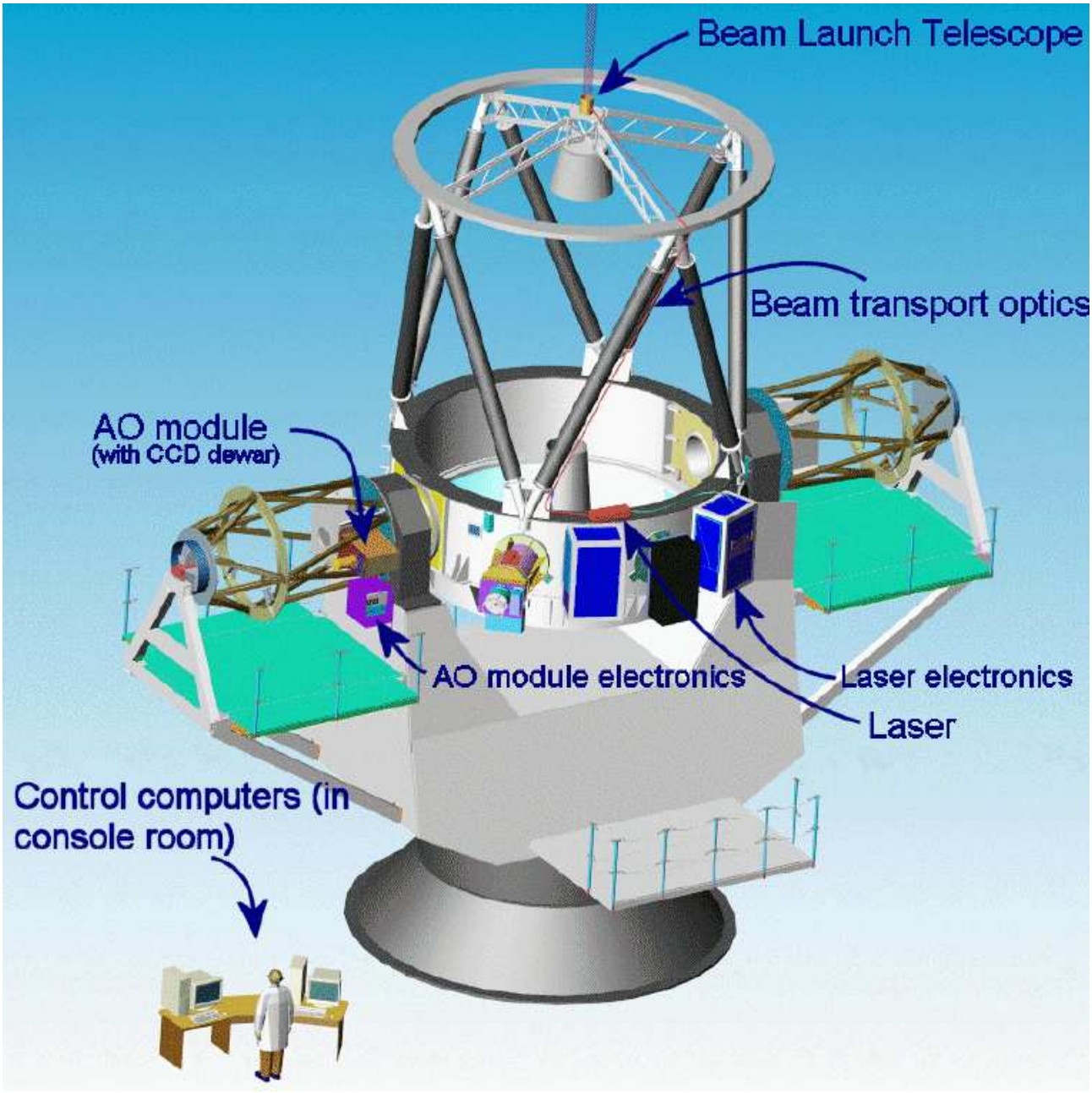


Figure 1: Overview of installation of SAM on the SOAR telescope.

sub-systems on the basis of their functionality and physical separation. Those sub-systems, and a first-level breakdown are listed here:

- SAM main module:
  - Deformable mirror

  - Wavefront sensor (either for NGS or for LGS)
  - Optical train
  - Calibration/simulation tools
  - Tip-tilt sensors
- Laser guide star:
  - Laser
  - Beam transfer optics
  - Laser launch telescope
  - Beam control system
- Control System
- Science Instruments
  - SAM Imager (SAMI)
  - Visitor Instrument
  - Visitor filter
  - High-resolution camera (HRcam)

Major instrument parameters are gathered in Table 1.

Table 1: SAM: major instrument parameters

| Sub-system | Description |
|---|---|
| Deformable mirror | Bimorph BIM-60 (Cilas), pupil 50mm, 60 electrodes |
| Wave-front sensor | Shack-Hartmann 10x10, CCD-39, $0\farcs41$ pixels in $3\farcs3$ sub-apertures |
| Re-imaging optics | Two OAPs $F = 810$ mm, off-axis shift 213.3 mm |
| Laser | DS20-355 (Photonics), tripled Nd:YAG, $\lambda = 355$ nm, 8W, 10 kHz |
| Laser Launch Telescope | $D = 0.3$ m, reflecting, behind the SOAR secondary, $H = 6.2...15$ km |
| Range gating | KD*P longitudinal Pockels Cell + two $\lambda/4$ plates and polarizers |
| Tip-tilt guiding | Two probes linked by fibers to APDs, $R_{lim} = 18$ |
| Focal plane | $3'$x$3'$ square field, $f/16.5$, scale 3 arcsec/mm, $R_{curv} = -0.9$m |
| CCD imager | 4Kx4K, $0\farcs05$ pixels, 6 filters |
| Collimated space | 50-mm beam, 100mm along axis |

In the initial phase, SAM will work without laser, using a bright ($< 12^m$) natural guide star (NGS). This operational mode permits full commissioning of the AO module and interesting science. The correction on-axis will be diffraction-limited in the visible (with moderate Strehl ratio but full resolution), opening an unexplored science niche. However, even at large off-axis distances the ground layer will still be corrected with the NGS, permitting the same kind of science as in the final SAM configuration in the regions of sky like Galactic plane where the chances to find a bright NGS are high.

# 3 SAM main module

The initial SAM concept was based on an electrostatic deformable mirror (DM) with a 35-mm pupil. We studied and rejected this DM for its insufficient stroke and fragility. A more classic, bimorph DM from CILAS has been purchased. This DM is reliable and has more than enough stroke[26] (it is used with 8-m telescopes). We were then forced to re-consider the optical design and selected finally a traditional re-imaging scheme with two off-axis paraboloidal (OAP) mirrors[21]. Thus, SAM transmits the original SOAR focal plane 1:1, without changing image scale or exit pupil location. It can "serve" standard SOAR instruments.

## 3.1 Optical design

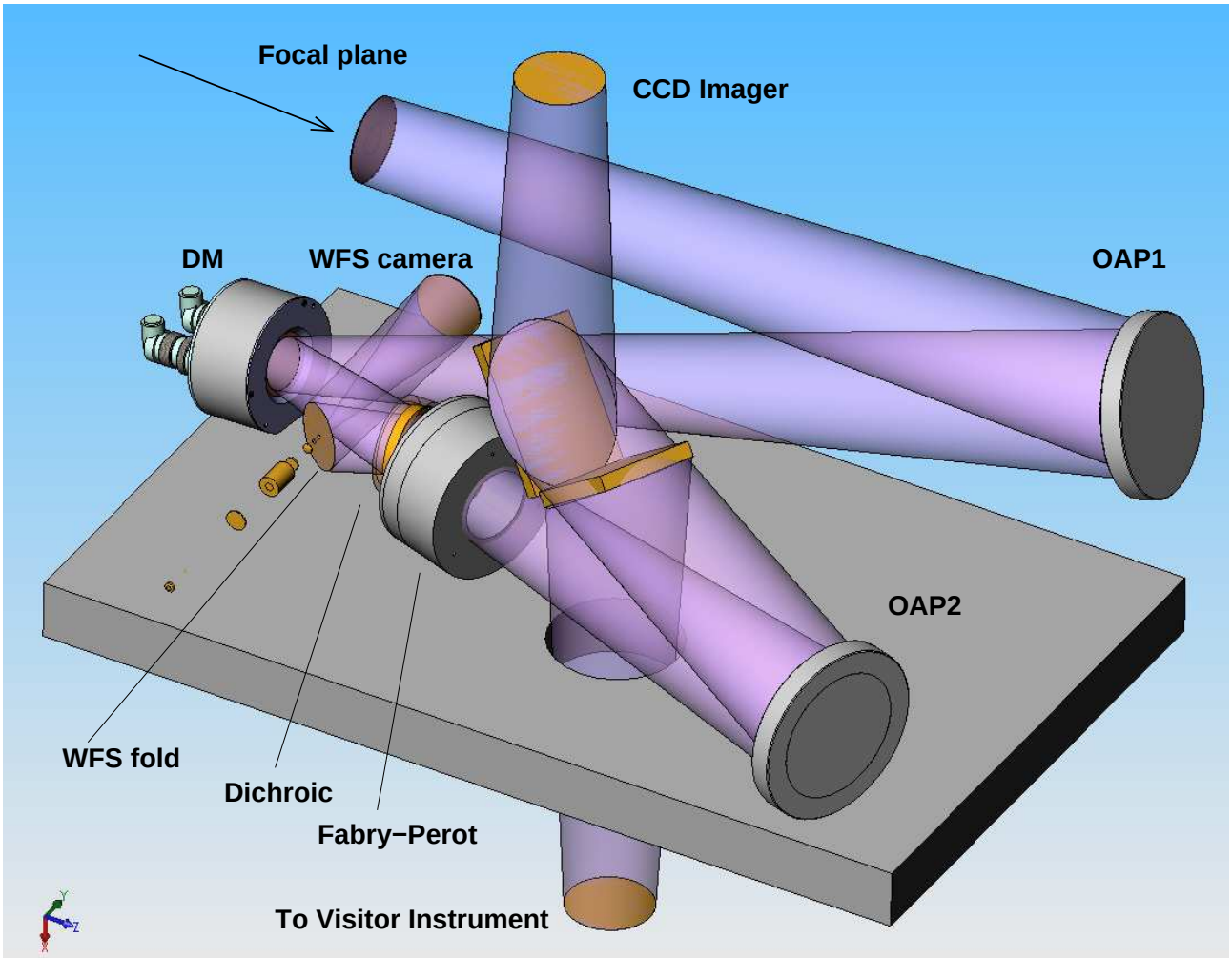


Figure 2: Optical layout of SAM. The beam size is exaggerated in this Figure.

The design with 2 OAPs has relatively few free parameters, as soon as the telescope and DM

diameter are fixed. We took care to optimize the layout in order to achieve a best match between optics and limited space available to SAM [25]. At the same time, many optical elements are placed in one common plane, parallel to a notional optical table (Fig. 2). The entrance beam is displaced inside the SOAR ISB[1] by 67.5 mm in order to bring the input focal plane further out (otherwise the DM would touch the ISB).

The parallel beam collimated by OAP1 is reflected by the DM and then split by the dichroic between science and WFS channels. The dichroic will be neutral for the NGS and will reflect 355 nm laser light for LGS. Right behind the dichroic, a portion of the collimated beam is available for installation of user-specified filters or a Fabry-Perot etalon. An atmospheric dispersion corrector (ADC) will be installed in the same space (it is not needed with narrow-band filters). Then the beam is re-focused by OAP2 and is directed either upwards to SAMI or downwards to the visitor instrument (VI). The switch from SAMI to VI is done by inserting a second fold mirror in the beam.

The WFS channel consists of a flat fold mirror with a hole at its center and a fast $F/4.5$ parabolic camera mirror. Following the WFS focus, small refractive optics will re-shape the beam and deliver it to the lenslet array (LLA) forming Shack-Hartmann spots at the WFS detector – CCD-39 camera [22]. The fused-silica LLA with suitable parameters (UV-transmitting) has been selected and purchased. The small WFS optics is straightforward in the case of NGS, but a somewhat different design for LGS is needed, so we are implementing the NGS and LGS options separately. In the case of LGS, we have to provide a collimated beam of suitable diameter that can be efficiently gated by the Pockels cell shutter. Also, we have to correct some spherical aberration and coma produced by the defocused (low-altitude) LGS as it goes through SAM optics. These requirements are fulfilled by our current optical design. WFS can be reconfigured for LGS range from 6.2 km to 15 km. This flexibility permits optimizing SAM parameters, after accumulating experience with this instrument. LGS height cannot be changed rapidly, however.

Table 2: Throughput of the SAM optics

| Science channel (450-900 nm) | | | WFS channel (355 nm) | | |
|---|---|---|---|---|---|
| Element | Spec | Goal | Element | Spec | Goal |
| OAP1 | 0.97 | 0.98 | OAP1 | 0.85 | 0.88 |
| DM | 0.98 | 0.98 | DM | 0.88 | 0.88 |
| Dichr. | 0.95 | 0.95 | Dich. | 0.95 | 0.97 |
| OAP2 | 0.97 | 0.98 | WFS fold | 0.88 | 0.95 |
| Fold | 0.97 | 0.98 | WFS cam. | 0.88 | 0.95 |
| Total | 0.85 | 0.88 | Total | 0.55 | 0.68 |

We give in Table 2 the SAM throughput as per optics specification and, alternatively, goal values if manufacturers exceed the specs. For the DM, the actual parameters are given. We believe that coatings on other elements can be at least as good as on the DM, and that the goals are hence realistic. Exceeding the specs is particularly critical for the LGS channel.

[1]ISB = Instrument Selector Box

### 3.2 Tip-tilt guiders

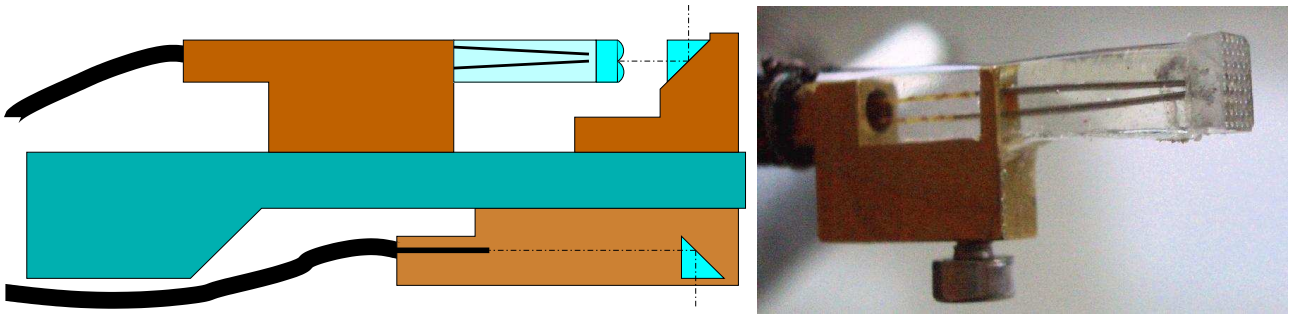

Figure 3: Arm of the tip-tilt guide probe. Light from the telescope is reflected by the upper micro-prism and falls onto lenslets, to be focused on fiber ends. The lower prism launches a test beam into the instrument. The photograph of the LLA+fiber prototype assembly is shown on the right.

When SAM works with LGS, the tip and tilt (t-t) have to be sensed on a NGS. One NGS is not enough, as it will cause appreciable variation of the compensated PSF in the field due to residual tilt anisoplanatism. Our trade study has shown that two t-t NGS are already sufficient, so the number of guide probes has been reduced from 3 to 2. The probes are located in the first (un-corrected) focal plane, and t-t correction is done by the SOAR fast tertiary mirror M3, as for other SOAR instruments. It means that tilts produced by the DM remain un-measured. We will eliminate these tilts in the control algorithm.

Guide stars will be normally selected outside the science field, in the patrol zone of $5'$ diameter around it. However, some science programs will require smaller FoV, and then selecting NGS closer to the science target will produce better results. Guide probes can move up to the center of the FoV, if needed. They are located close to the focal plane and produce only small vignetting (estimated probe width is $10''$ on the sky). In addition to positioning in 2 coordinates, probes can be focused within a small ($\pm 3$ mm) range, to allow for focus adjustments in the science instruments.

The guide probe consists of a 2x2 lenslet array (LLA) that splits the stellar image into 4 quadrants. Light from each quadrant is focused onto a fiber end (core diameter 100 $\mu$m), to be conducted to a photon-counting avalanche photo-diode (APD). We will use modules with 4 APDs from Perkin Elmer (SPCM-AQ4C). Initially, a quadrant photo-multiplier had been considered as an alternative, but we opted for APDs because of their higher quantum efficiency in the red [13].

The coupling between fibers and LLA has been successfully prototyped [24]. The LLA has a pitch of 0.5 mm, i.e. a field-of-view of $3''$ for the probe. The focal length of the LLA, 1.2 mm, is short enough to focus the $F/16.5$ SOAR beam to a circle of 73 $\mu$m diameter that fits into the fiber core. Each fiber is aligned individually with respect to the LLA before the assembly is glued into a single solid block. This tiny block is mounted at the end of the guide probe (Fig. 3) and fed by a telescope beam folded with a micro-prism, without any magnification. On the down-looking side of the probe, we plan to install another prism that projects a point source (single-mode fiber) into the SAM instrument. These sources, controlled in position and focus by the guide-probe motions, will be very useful for various instrument checks (e.g. to measure non-common-path errors), as well as for visualizing the guide-probe positions in the science field.

### 3.3 Mechanical design

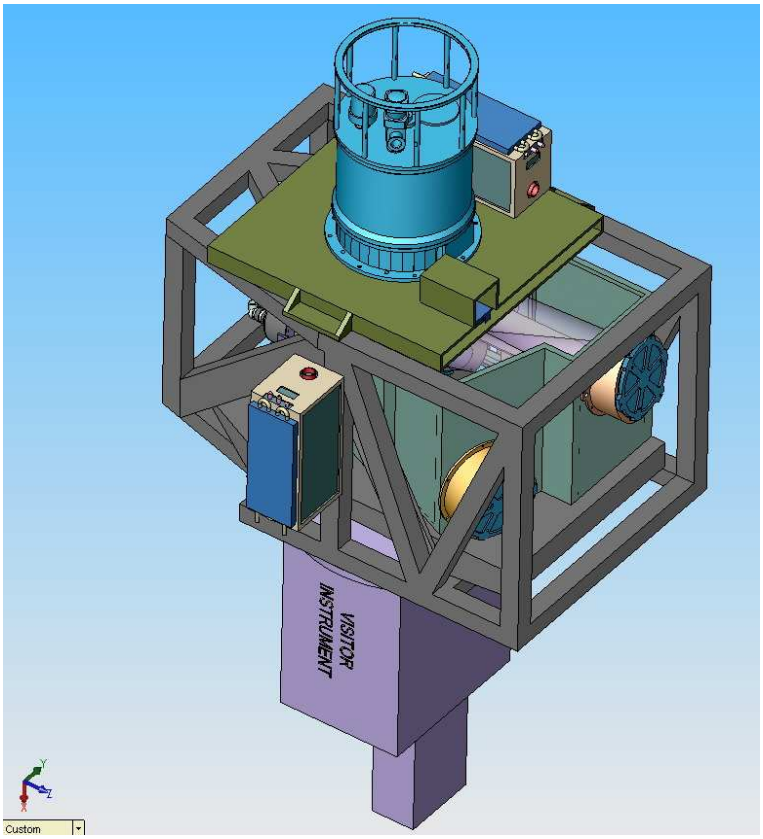


Figure 4: SAM in its support frame, with VI and SAMI. The frame is mounted to the SOAR ISB (to the left, not shown).

All optical elements of SAM are mounted on a rigid structure, called *bench*. The bench is mounted kinematically inside a frame structure that connects it to the SOAR ISB (Fig. 4). Visitor instrument (VI) is attached to one side of the frame, and SAMI to another side. Such design permits to de-couple the bench from frame mechanically, so that flexure and thermal deformations of the steel frame do not distort the bench. At the same time, the coupling between frame and bench is rigid enough to assure that image in the focal plane of VI and SAMI is not displaced as SAM rotates together with Nasmyth bearing.

The design of the optical bench (Fig. 5) is based on a custom-made rigid aluminum-alloy table. A box-type structure connects the table to the optical cells and increases the overall rigidity of the bench. The space in front of the first wall is quite crowded: it hosts two guide probes with their stages, the DM, the WFS fold and camera mirrors, and the WFS itself with its CCD-39 detector. The dichroic is parallel to the front wall.

The fold mirror directing the beam to VI moves vertically on a linear stage, to be either retracted or placed into the beam. Similar linear stages are used for focusing the WFS camera mirror and for the guide probes. The user filter (Fabry-Perot) will move in and out of the beam on a stage, too.

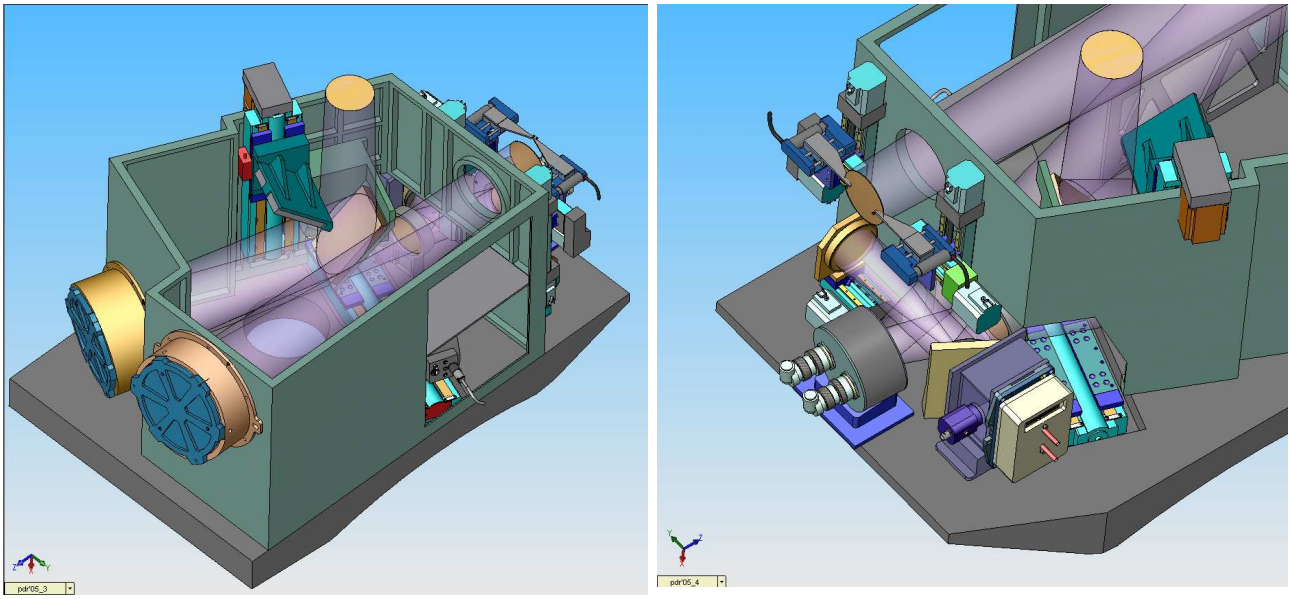

Figure 5: SAM optical bench. Left – view from the OAP side, right – view from the front side.

A first-order analysis of the SAM flexure shows it to be 4 times smaller than required. We are thus confident that flexure specifications can be met.

### 3.4 Turbulence simulator

SAM will include a small built-in turbulence simulator, TurSim. It is based on two rotating glass disks with phase distortions approximating atmospheric turbulence [5]. TurSim will project its light onto the optical axis of SAM with a small flip mirror. It will be focused initially to infinity (NGS operation), then to the selected LGS height. The light source will be, respectively, either a red diode laser or a UV LED. TurSim will permit a quick check of AO loop during daytime or for troubleshooting. We are already using this tool in the prototype work, as an essential element in software development and testing. Work on the SAM laboratory prototype is presented separately [20].

## 4 Laser guide star

SAM will use an 8 W pulsed, frequency-tripled, Nd:YAG laser. Its short wavelength of 355 nm is doubly advantageous. First, the photon flux from Rayleigh scattering increases as $\lambda^{-3}$ and, second, this radiation does not present visual hazards. The UV RLGS is aircraft- and satellite-safe, obviating any need for coordination of AO observations with external agencies. The narrow laser beam on its way to the launch telescope needs to be shielded, but once it leaves the Laser Launch Telescope (LLT) it will be safe.

The laser (Table 3) is a rugged industrial model with a nominal time between failures of 8000 hours. No adjustments are required in normal use. The LLT will always point on telescope axis and will be focused at a fixed distance (to be optimized in the range 6.2 km to 15 km). Fine tuning of the

Table 3: Parameters of the DS20-355 laser from Photonics

| | |
|---|---|
| Wavelength | 355 nm |
| Average power at 10 kHz | 8 W |
| Pulse width | 40 ns |
| Beam diameter | 0.9 mm |
| Beam divergence | 1.4 mrad |
| Beam quality | Single $TEM_{00}$ mode |
| Cost | 138 000 USD |
| Laser head size | 191x600x127 mm |
| Laser head weight | 17 kg |
| Electrical power | 110V 20 Amps |

LGS position on the sky (for flexure compensation) will be done by a remotely controlled pointing of the LLT. We expect that a major part of the pointing error will be caused by elastic flexure and thus will be predictable.

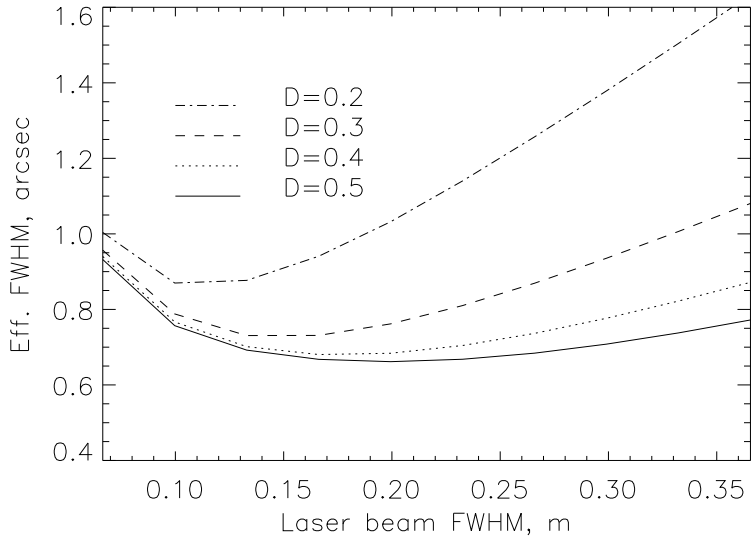


Figure 6: Effective laser spot size $\beta_e = \beta/\sqrt{T}$ as a function of the FWHM width of laser beam and the LLT diameter $D$, in case of $0''.67$ ground seeing.

We computed the Full Width at Half Maximum (FWHM) $\beta$ of the laser spots distorted by the ground-layer turbulence on upward and downward propagation (because of the beam convergence, only low layers effectively contribute to the image spread) [14]. The *effective* image size $\beta_e = \beta/\sqrt{T}$ takes into account the transmission $T$ of the LLT resulting from the truncation of the Gaussian beam by its circular aperture (neglecting central obscuration). We expect the centering errors in the WFS

to be proportional to $\beta_e$, so this is the parameter to minimize as function of LLT diameter $D$ and of the FWHM $L$ of the laser beam projected onto the LLT aperture.

The results are shown in Fig. 6 for a typical expected ground-layer seeing. We see that a gain in increasing LLT diameter above 30 cm is small, but selecting a 20-cm LLT entails a non-negligible increase in the spot size, hence in the required flux. Note that achieving sub-arcsecond spot size with LGS remains a challenge for the current generation of LGS-AO systems. We will try to reach the spot size predicted by Fig. 6.

Another trade study [15] concerns selection of an optimum range gate [15]. As it is increased, the spots "seen" by sub-apertures near the edge of the pupil become radially elongated. Selecting a range gate that avoids such elongation has been a baseline choice, but it is not optimum. Some elongation is actually required for minimizing the wavefront errors because the benefit of increased flux out-weighs the elongation. Optimum elongation calls for peripheral spots to be ∼3 times longer than their width. For a 10-km LGS this corresponds to a range gate of 460 m.

By extrapolation from the published value of the return flux in the RLGS AO system at Starfire Optical Range (Ch. 12 in Ref. [3]) we estimate that the WFS will detect over 300 photo-electrons per sub-aperture per 2 ms loop time if the range gate is set to 460 m and LGS is at 10 km altitude. A calculation by S. Thomas[2] based on Rayleigh scattering cross-section and realistic assumptions on instrument transmission gives LGS flux several times higher.

Range-gating will be done in the WFS by means of a Pockels cell, like in other RLGS AO systems. An alternative solution would be to use a "fast" CCD detector with substrate gating developed at Lincoln Labs [2]. We contacted the developers of these CCDs and the AO group at the Arizona University that uses them, and made a comparative study of those two options. Gated CCDs turned out to be a more expensive, single-vendor product with potentially low (40% or less) quantum efficiency in the UV. Thus we confidently selected CCD-39 with Pockels cell [11]. Our delivered CCD-39 camera has a QE of 73% at 355 nm.

The LLT will be located behind the secondary mirror of SOAR. This is the best position for many reasons. One of those is the effective blocking of the strong scattered signal from low altitudes. The entrance aperture of the WFS will not transmit the highly-defocused return beam because it will fall within the central obscuration zone. Only when the laser "bullet" is close to its nominal altitude the light will enter the WFS. Even a moderate (<10%) rejection ratio of the range-gate shutter will be sufficient for obtaining compact and high-contrast spots.

The secondary mirror assembly of SOAR is relatively small and light-weight (80 kg), which places tight constraints on the LLT design. We plan using a light-weight 30-cm mirror with a small secondary suspended on vanes. The primary will be actuated in tip, tilt and focus. The laser will be located on the upper surface of the telescope elevation ring. Its beam will be transmitted to the LLT over a distance of $\sim$ 8 m with 2 or 3 reflections by flat mirrors. Owing to the relative stiffness of the SOAR tube (total flexure less than 0.5 mm), it will be possible to transmit the beam to LLT without controlling the tilts of those mirrors.

We plan to proceed with the optical design of the LLT and beam-transfer optics. We will also evaluate an alternative option of locating the LLT near the SOAR primary, to avoid beam transfer and simplify the LLT design (at a cost of reduced range gate and return flux and increased scattered light). The concept of beam control is not yet developed. It will involve monitoring laser output

[2]S. Thomas, "A study of adaptive optics for the visible range". PhD thesis, Nice University, 2005

power, beam centering in the LLT aperture and beam optical quality.

# 5 Control system and software

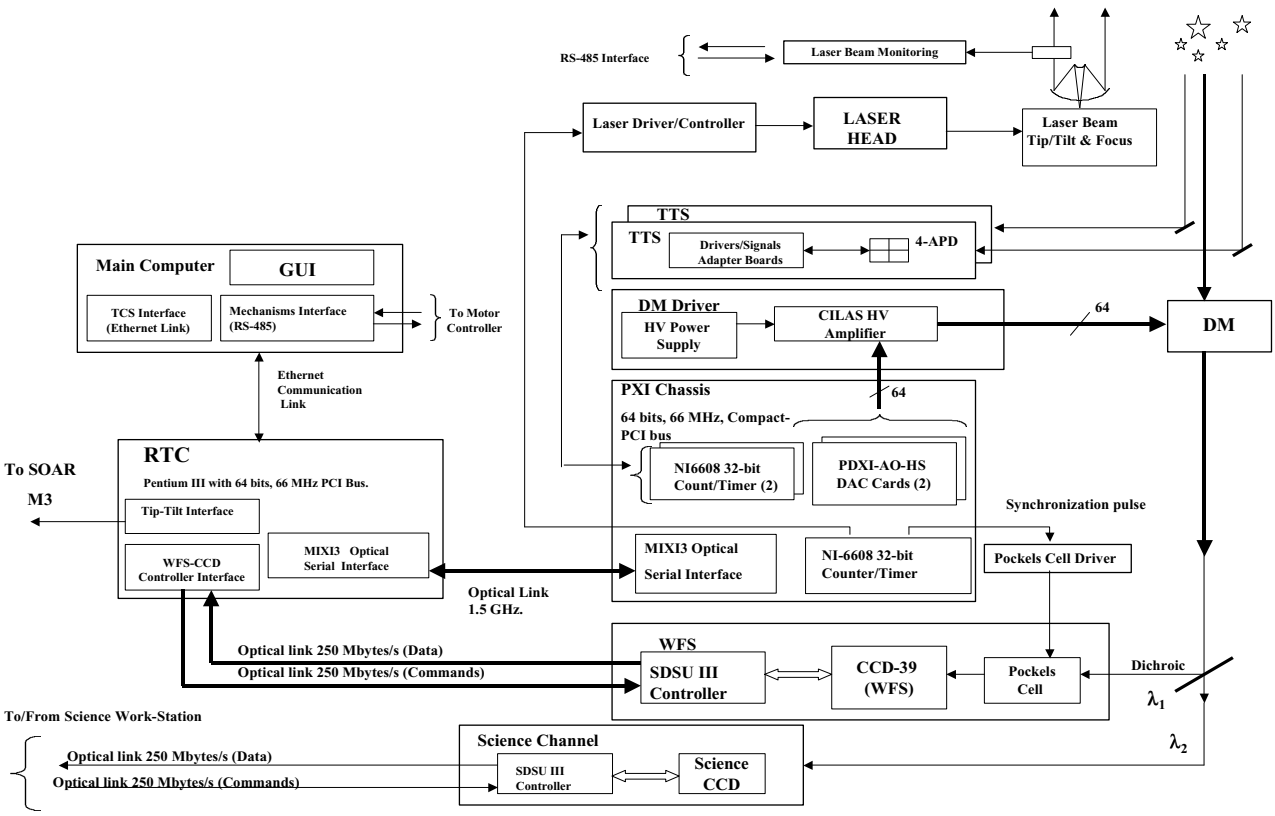


Figure 7: Block diagram of SAM electronics and control system.

The SAM control system has been designed to make it easy to take advantage of existing modules as much as possible. The use of Linux and the SDSU detector controller means significant overlap and synergy with other SOAR software. We use, mostly, commercially available, inexpensive processors, chassis and controller modules in SAM (Fig. 7).

A significant part of the SAM control system and software is already implemented and tested [30]. We were able to close the loop in the laboratory prototype using the actual Real-Time Computer (RTC) connected to the PXI chassis, the actual DM and the WFS camera with CCD-39 [20]. Some problems in interfacing RTC to the Generation-III SDSU controller have been encountered and solved, in close interaction with the team of R. Leach who fabricated and tested our camera system prior to

delivery. Details of SAM real-time software, its user interface, and the results of tests are described in separate documents.

The SAM will incorporate a large number of mechanisms, both in the main module and in the LGS. In the interest of modularity and simplifying trouble shooting and maintenance, we prefer to use motors and actuators which have their own local intelligence [29]. The connections to the controlling computer is via a generic, serial, networking system, employingg the RS-485 protocol. The control system is LabView based (SOAR standard), which enables us to build on our now extensive experience with this architecture. For example, control software of SAMI will be, to large extent, a clone of the existing SOAR Imager software.

# 6 Science instruments and filters

SAM will contain a built-in CCD imager (SAMI). This decision has been taken because the regular SOAR imager is not available for AO-corrected focus, being located on the SOAR side-port. The SAM imager will be optimized for the red part of the optical spectrum where the SAM resolution gain is larger, while the regular SOAR imager works efficiently in the UV. At first, SAMI will use an existing CTIO dewar with a SIT CCD (24 $\mu$m pixels), until funds and manpower for the definitive detector are available.

The second, "visitor" port of SAM will host the SOAR Integral Field Spectrograph (SIFS). The SIFS pixels are $0\farcs3$ square, so this instrument will greatly benefit from the improved light concentration provided by SAM: its magnitude limit for point sources will be extended by approximately $1^m$.

In the future, other small, specialized instruments can be placed at the visitor port. During the initial phase of SAM, when it will work without a LGS, a small **high-resolution camera** will occupy the visitor port, offering diffraction-limited resolution on bright targets that will also serve as guide stars. Our concept of HR-camera is based on the ST-10 CCD with a commercial filter wheel and a single-lens focal extender that ensures good sampling of diffraction-limited images (15 mas pixels) [23].

**Collimated space** is available for installation of user filters. The space is quite tight, limiting the maximum size of the filter. The diameter of the collimated beam is 50 mm, but the beam footprint is larger, depending on the FoV size. Current SAM design is compatible with the ET70 Fabry-Perot etalon from IC Optical Systems (outer diameter 153 mm, thickness 75 mm, beam diameter 70 mm). A filter as thick as 100 mm can be used, but with a smaller outer diameter.

SAM contains a mechanism for quick removal and insertion of the filter in the beam. We believe that such capacity is essential for calibrating narrow-band observations and for achieving flexibility of SAM use. When the filter is in the "out" position, it can be accessed and removed (or changed) without dismounting SAM from telescope. Filter access will be possible only during daytime. Details of such access are still being worked out. For wide-band imaging, the place in the collimated space will be occupied by the atmospheric dispersion corrector (ADC). We prefer to provide a special, small ADC for SAM rather then rely on the future trombone-type ADC promised by SOAR because the latter will displace the beam, entailing problems with LLT pointing.

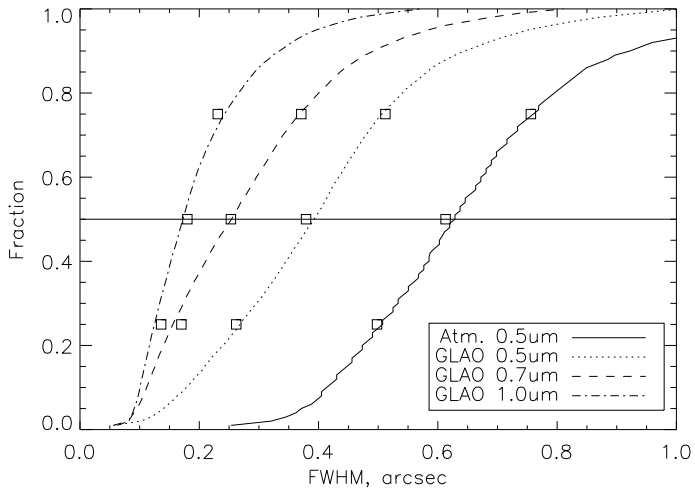


Figure 8: Cumulative distributions of the un-compensated FWHM image size at 0.5 $\mu$m and SAM-compensated FWHM at three wavelengths. The values derived from the OTP models are plotted as squares.

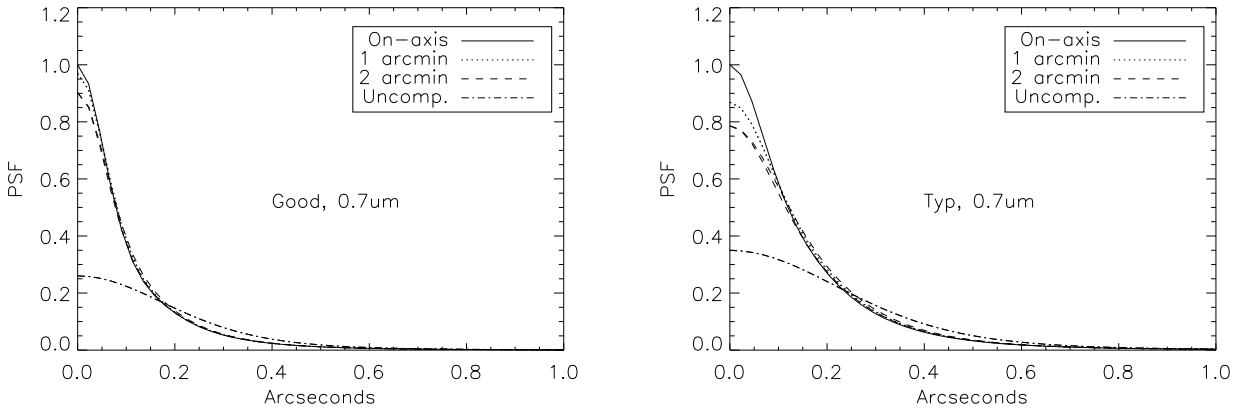


Figure 9: Cuts of the PSFs in two directions, $x$ and $y$, in the field center and at 1 and 2 arcmin. radii, wavelength 0.7 $\mu$m. Left: good conditions, right: typical conditions, observations at zenith. Un-compensated PSFs are plotted for comparison.

# 7 Performance and error budget

Estimates of SAM performance and gain over un-compensated seeing have been considerably improved for two reasons. First, we now know better the instrument parameters of SAM. Its combination of DM and WFS results in effective compensation of ∼45 Zernike modes, not 66 as believed initially. Tip-tilt sensing is assumed to be done on two NGSs at opposite edges of the patrol field, at 2.5′ radius from the center. Second, we have a much better data on turbulence vertical profile at Cerro Pachón [9]. The MASS-DIMM site monitor has been installed in a tower 6 m high and began regular operation in December 2004. We have processed some 6500 individual optical turbulence profiles (OTP) and were able to derive OTP models representative of good (25% quartile), typical (median) and bad (75%

quartile) conditions. We now take into account the finite outer scale of turbulence in the calculations. Two alternative techniques of PSF calculation have been used, and they give concordant results [17].

We processed all individual OTPs and computed statistical distributions of FWHM resolution with SAM at three wavelengths, at zenith (Fig. 8). The gain in resolution is impressive even at 0.5 $\mu$m (1.6 under median conditions), and remains interesting under bad conditions as well. We can confidently affirm that SAM will significantly improve the image quality during at least 75% of nights. The gain in resolution is reduced only slightly (e.g. 1.6 to 1.45) for observations at a realistic zenith distance of 50°. Moreover, we show that our OTP models are indeed representative of good, typical, and bad conditions.

Figure 9 shows the cuts through the SAM-compensated PSF at the center of the FoV and in two off-axis positions. Two cuts (in $x$ and $y$) are over-plotted to evaluate PSF asymmetry, but they are practically overlapping. More detailed study of the PSF uniformity and asymmetry is given in [7, 8].

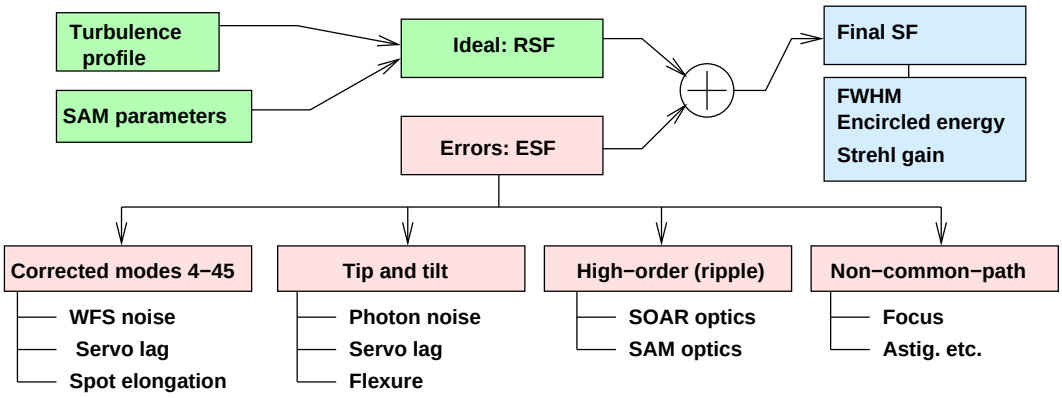


Figure 10: Top-level error budget diagram.

Performance of a real SAM instrument on the real SOAR telescope will be somewhat degraded from the ideal. We studied the influence of various instrumental imperfections on the final PSF and formulated an *error budget* [18] that constrains these errors at a reasonably small level. This is the first time such a budget for a GLAO system has been presented. The error budget of a classical AO system is formulated in terms of residual rms wave-front aberrations that translate directly to Strehl ratio. For a GLAO system, the goal is to improve the PSF, hence this metric is inappropriate and a new method is needed.

The "top-down" approach to the error budget is taken here: we set some acceptable level of performance degradation and try to fit the errors into this allocation. Eventually, a "bottom-top" analysis will be performed, starting with the parameters of the individual sub-systems and working out their combined contribution.

All instrument errors increase the residual wavefront errors in additive way. We define an *error structure function* (ESF), to be added to the ideal residual structure function (RSF) before calculating OTF and PSF, as depicted in Fig. 10. Both RSF and ESF are increasing functions of distance; it turns out that RSF is almost a linear function. We specify the error budget by constraining ESF to be no more than 10% of RSF under typical conditions. This ensures that instrumental errors degrade resolution by 10%, approximately. The comparison between RSF and ESF is done for a specific

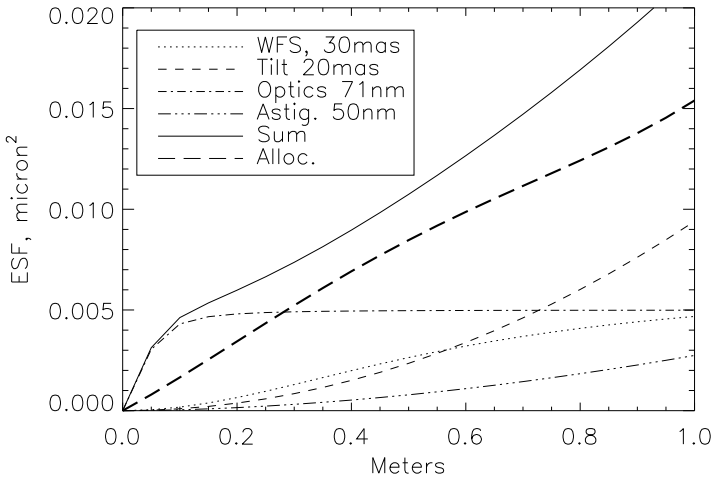


Figure 11: Different components of the ESF and their sum (solid line). The thick long-dash line marks our allocation (10% of RSF for typical conditions).

Table 4: Error budget

| Error | Parameter | RMS error at 0.5m base, nm |
|---|---|---|
| Corrected modes | Spot rms error 30 mas | 51.3 |
| Tip and tilt | Tilt rms error 20 mas | 48.4 |
| Static high-order aberrations | $70.7/\sqrt{2}$ nm rms | 70.5 |
| Non-common-path errors | Astigmatism 50 nm rms | 28 |
| Total | - | 104 |
| Allocation | 10% | 92 |

distance of 0.5 m, because at this baseline the influence of the ESF on the PSF is most pronounced. However, we also consider full functions and compute the effect of instrument errors on the PSF.

The ESF is a sum of individual contributions (Fig. 10). Each contribution is studied and modeled separately, then a total error budget is compiled. One unexpected result of this study is that the ESF caused by high-frequency optical imperfections of SOAR (ripple) is a major contributor (Fig. 11) [27]. The reason can be traced to the very small spatial scale of the ripple produced by a small optical tool. The absolute amplitude of the ripple is actually quite small, well within the specifications for SOAR and at the state-of-the art level of astronomical optics. We are forced to exceed slightly our 10% allocation for ESF because of optical errors. However, the effect of these errors on the final SAM performance remains small (Table 4).

Table 5: Estimates of PSF parameters: uncorrected with ideal telescope, uncorrected with real SOAR optics, with budgeted SAM errors and for the ideal SAM instrument. Observations at zenith, wavelength 0.7 $\mu$m.

| Parameter | FWHM, arcsec | | | Energy in 0.3″ diam. | | |
|---|---|---|---|---|---|---|
| Case | Good | Typical | Bad | Good | Typical | Bad |
| Atmosphere only | 0.449 | 0.554 | 0.684 | 0.203 | 0.143 | 0.099 |
| Atm. + SOAR opt. | 0.452 | 0.559 | 0.692 | 0.180 | 0.127 | 0.089 |
| SAM, errors | 0.200 | 0.282 | 0.396 | 0.301 | 0.218 | 0.150 |
| SAM, ideal | 0.170 | 0.254 | 0.371 | 0.380 | 0.272 | 0.185 |

# 8 Summary of SAM project progress

A progress of the SAM project since the Conceptual Design Reviews (April 7, 2003 and January 26, 2004) is resumed shortly. The system requirements [10] did not change significantly since 2004.

Table 6: Summary of SAM progress.

| Category | Activity | Reference |
|---|---|---|
| Procurement | Deformable mirror BIM-60 with HV driver | [26] |
| | WFS camera CCD-39 and SDSU-III controller | [11] |
| | Lenslet array | [22] |
| | Real-time computer | [30] |
| | Main optics (bids obtained) | [21] |
| Trade studies | Pockels cell vs. gated CCDs | [11] |
| | Tip-tilt sensor: PMT vs. APD | [13] |
| | Optimum range gate | [15] |
| | Number and magnitude of t-t stars | [12] |
| | LLT diameter optimization | [14] |
| | Improved performance prediction | [17] |
| | Error budget | [18] |
| Designs | Optical layout optimized | [25, 19] |
| | WFS-NGS and WFS-LGS designs | [22] |
| | Mechanical design: bench and frame | [11] |
| Software | Design of control algorithm | [16] |
| | Real-time software coded and tested | [30, 20] |
| Prototyping | Closed the loop with real DM and WFS | [20] |
| | Tip-tilt fiber coupler | [24] |

## References


[1] V.L. Krabbendam, T.A. Sebring, and S. Heathcote, "Southern Astrophysical Research Telescope (SOAR): steps on the road to success", *Proc. SPIE,* **4837**, pp. 71-81, 2003.

[2] R.K. Reich, R.W. Mountain, W.H. McGonagle et al., "Integrated electronic shutter for back-illuminated charge-coupled devices", *Trans. IEEE Electr. Dev.,* **40,** pp. 1231-1237, 1993.

[3] F. Roddier, ed., *Astronomical Adaptive Optics,* Cambridge Univ. Press, Cambridge, 1999.

[4] R.G.M. Rutten, P. Clark, R.M. Myers et al., "Facility class Rayleigh beacon AO system for the 4.2-m William Hershel Telescope", *Proc. SPIE,* **4839,** pp. 360-369, 2003.

[5] S. Thomas, "A simple turbulence simulator for adaptive optics", *Proc. SPIE,* **5490**, pp. 766-773, 2004.

[6] A. Tokovinin, B. Gregory, H. Schwarz, "Visible-light AO system for the 4.2-m SOAR telescope", *Proc. SPIE,* **4839,** pp. 673-680, 2003.

[7] A. Tokovinin, "Seeing improvement with ground-layer adaptive optics", *Publ. Astron. Soc. Pacif.,* **116**, pp. 941-951, 2004

[8] A. Tokovinin, S. Thomas, B. Gregory, N. van der Bliek, P. Schurter, R. Cantarutti, E. Mondaca, "Design of ground-layer turbulence compensation with a Rayleigh beacon", *Proc. SPIE,*, **5490**, pp. 870-878, 2004.

[9] A. Tokovinin, T. Travouillon, "Model of optical turbulence profile at Cerro Pachón", *MNRAS,*, accepted, 2005.


**System design notes:**


[10] Functional and performance requirements of SAM. October 26, 2005.

[11] SAM-AD-02-1101, "Gated CCDs vs CCD-39 and Pockels cell", May 5, 2004

[12] SAM-AD-02-1103, "How many tip-tilt stars for SAM?", March 25, 2004

[13] SAM-AD-02-1104, "Limiting magnitude for tip-tilt correction", April 2, 2004

[14] SAM-AD-02-1105, "Laser Launch Telescope Diameter and Return Flux" May 14, 2004

[15] SAM-AD-02-1106, "Optimum spot elongation in SAM", February 16, 2005

[16] SAM-AD-02-1107, "Control loop of SAM: modal control", March 7, 2005

[17] SAM-AD-02-1108, "PSF calculation for SAM", May 17, 2005

[18] SAM-AD-02-1109, "SAM error budget", May 26, 2005

[19] SAM-AD-02-1110, "SAM Optical bench: table-type or box-type", August 21, 2005

[20] SAM-AD-02-1301, "Closed-loop experiments with SAM prototype", May 2, 2005

[21] SAM-AD-02-2201, "SAM Optical Design", August 25, 2005

[22] SAM-AD-02-2202, "WFS Optics With Collimated Beam", March 14, 2005

[23] SAM-AD-02-2204, "High-resolution camera for SAM", March 15, 2005

[24] SAM-AD-02-2205, "Optical concept of tip-tilt sensor", October 26, 2005

[25] SAM-AD-02-2206, "Notes on SAM Optical Layout", August 18, 2005

[26] SAM-AD-02-2304, "Influence functions of BIM-60", March 14, 2005

[27] SAM-AD-02-2305, "Quality of SOAR optics", May 25, 2005

[28] SAM-AD-02-3301, "Support cage trade analysis", March 4, 2004

[29] SAM-AD-02-5230, "Motion Control Design: Overview", March 16, 2005

[30] SAM-AD-02-8211, "Real-Time Computer Software", June 10, 2004